1. Intense phosphorescence

2. High thermal stabilities
(> 400 °C in N_2)

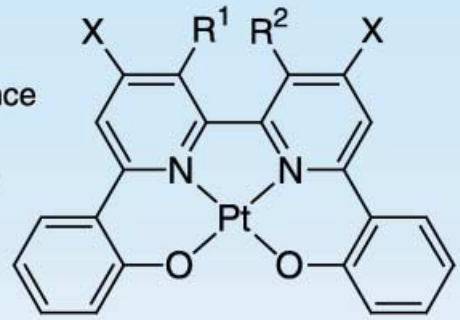

3. Promising PHOLED materials
(c.f. Alq_3, Znq_2)

Pt Complexes Bearing Tetradentate Quinolinolate-Related Chelates

$R^{1,2}$ = HC=CH
X = Ph

$R^1 = R^2 = H$
X = *t*Bu

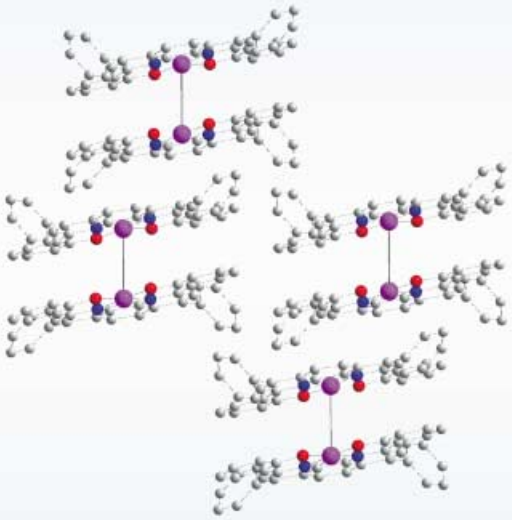

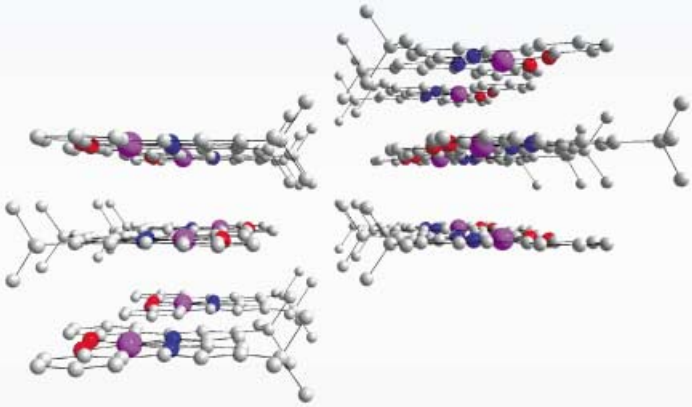

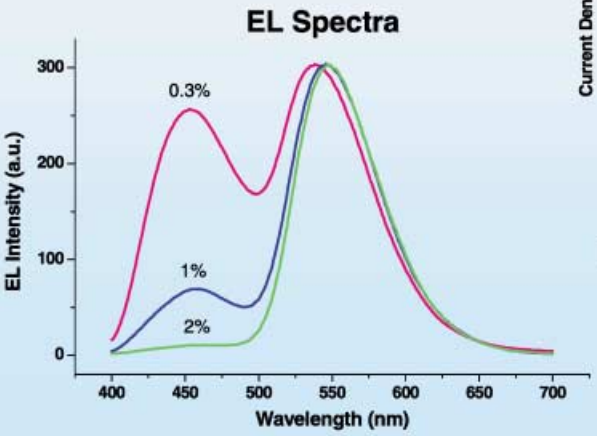

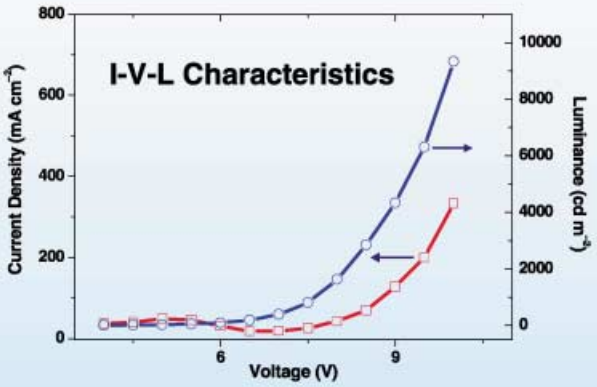

[ITO/NPB/**Pt**-doped (x%) $Bepp_2$/LiF/Al]

For more information see the following pages.

  0947-6539/03/0906-1263 $ 20.00+.50/0

Structural, Photophysical, and Electrophosphorescent Properties of Platinum(II) Complexes Supported by Tetradentate N_2O_2 Chelates

Yong-Yue Lin,[a, b] Siu-Chung Chan,[a] Michael C. W. Chan,[a] Yuan-Jun Hou,[a] Nianyong Zhu,[a] Chi-Ming Che,*[a] Yu Liu,[c] and Yue Wang[c]

Abstract: We present an examination of the structural and photophysical characteristics of [Pt(N_2O_2)] complexes bearing bis(phenoxy)diimine auxiliaries (diimine = 4,7-Ph_2phen (**1**) and 4,4′-tBu$_2$bpy (**2**)) that are tetradentate relatives of the quinolinolato (q) ligand. These neutral derivatives display high thermal stability (> 400 °C in N_2). While the crystal lattice in **1** consists of (head-to-tail)-interacting dimers, molecules of **2** are arranged into infinitely stacked planar sheets with possible π–π interactions but no close Pt···Pt contacts. Complexes **1** and **2** exhibit moderately intense low-energy UV/Vis absorptions around $\lambda = 400-500$ nm that undergo negative solvatochromic shifts. Both derivatives are highly luminescent in solution at 298 K with emission lifetimes in the μs range, and mixed ^{3}[l → π*(diimine)] (l = lone pair/phenoxide) and ^{3}[Pt(d) → π*(diimine)] charge-transfer states are tentatively assigned. The excited-state properties of **2** are also investigated by time-resolved absorption spectroscopy and by quenching experiments with pyridinium acceptors to estimate the excited-state redox potential. These emitters have been employed as electrophosphorescent dopants in multilayer OLEDs. Differences between the brightness, color, and overall performance of devices incorporating **1** and **2** are attributed to the influence of the diimine substituents.

Keywords: charge transfer · electroluminescence · N,O ligands · phosphorescence · platinum

Introduction

The pursuit of highly luminous and efficient electroluminescent (EL) materials with suitable chemical and operational stability has proliferated over the last decade, and commercialization of technologies based on organic light-emitting diodes (OLEDs) have resulted. More recently, intense efforts have been devoted to electrophosphorescent emitters because of the theoretical augmentation in device efficiency relative to established fluorescent OLEDs.[1, 2] Phosphorescent emitters containing heavy transition metals, which promote spin-orbit coupling, have the potential to harness both singlet (25%) and triplet (75%) excitons after charge recombination. In this regard, several accounts of platinum(II)[3, 4] and iridium(III)[5] complexes supported by organic ancillary ligands as dopants in small molecule- and polymer-based OLEDs have appeared, and exceptional device performances have been reported.[6]

Research into ligand design for EL materials has been dominated by the 8-hydroxyquinoline moiety, as in Alq_3.[7] Its use as an emissive and electron-transporting material has been widespread because Alq_3 combines many chemical and physical attributes that are requisite for such a function, including sufficient electron mobility, high photoluminescence (PL) quantum efficiency, and stability for vacuum deposition coupled with resistance to subsequent recrystallization of the amorphous film. Surprisingly, optimization studies involving systematic variation of the quinoline ligand structure have not proven particularly fruitful and have often afforded adverse device parameters.[8] Attempts to develop alternative q-containing metal complexes for EL applications

[a] Prof. Dr. C.-M. Che, Dr. Y.-Y. Lin, S.-C. Chan, Dr. M. C. W. Chan, Dr. Y.-J. Hou, Dr. N. Zhu
Department of Chemistry and HKU-CAS Joint Laboratory on New Materials
The University of Hong Kong
Pokfulam Road
Hong Kong SAR (China)
Fax: (+852) 2857-1586
E-mail: cmche@hku.hk

[b] Dr. Y.-Y. Lin
Department of Chemistry
Yunnan Normal University
Kunming 650092 (China)

[c] Prof. Y. Wang, Y. Liu
Key Laboratory for Supramolecular Structure and Spectroscopy of Ministry of Education
Jilin University
Changchun 130023 (China)

Supporting information for this article is available on the WWW under http://www.wiley-vch.de/home/chemistry/ or from the author.

0947-6539/03/0906-1264 $ 20.00+.50/0

have focused on the closest relatives of Alq_3, such as trivalent Ga, In, and Sc,[8, 9] as well as Znq_2 (or $(Znq_2)_4$).[10]

By integrating the two design features described above, we have prepared phosphorescent platinum(II) complexes ligated by tetradentate q-related auxiliaries N_2O_2 ($N_2O_2H_2$ = bis(2′-phenol)bipyridines and -phenanthrolines; Scheme 1) for employment as new dopants in EL devices. The N_2O_2 ligand framework is devised with chemically inert functionalities and the considerable chelate effect should ensure good thermal stability. Phenyl and *tert*-butyl substituents are appended to the $Pt(N_2O_2)$ moiety, since coordinatively unsaturated square-planar Pt^{II} compounds are known to engage in excited-state and exciton self-quenching reactions in solution[11] and EL devices,[12] respectively. The nature of these substituents may therefore yield emitting layers with different quenching behavior as well as other relevant physical properties. Both complexes have been structurally characterized and an assessment of their crystal packing arrangements is presented. Investigations into the performances of these emitters in OLEDs have revealed substituent-dependent electrophosphorescent energies and device characteristics.

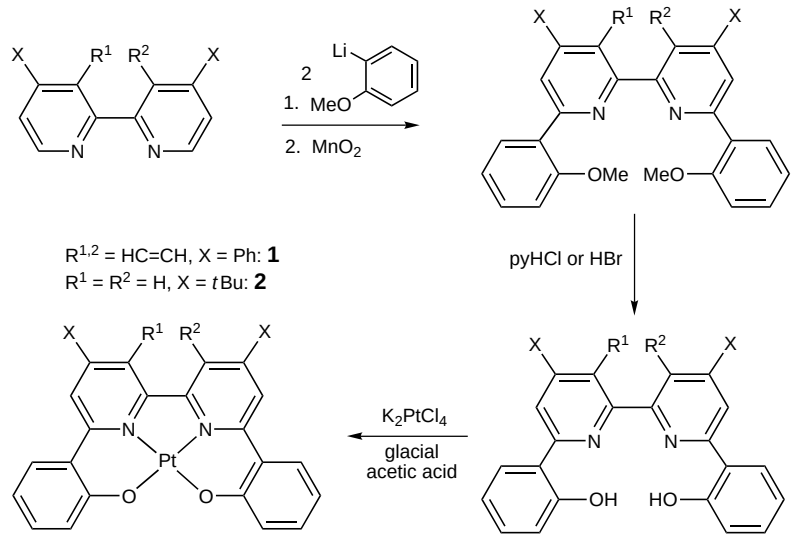

Scheme 1. Synthesis of **1** and **2**.

Abstract in Chinese:

本文報導了帶有喹啉(q)類四齒配體雙(酚氧基)-二亞胺絡合物 $Pt(N_2O_2)$ (二亞胺 = 4,7-Ph_2phen (**1**), 4,4′-tBu$_2$bpy (**2**))的結構和光物理性質。這些中性衍生物具有很高的熱穩定性(在氮氣下高于 400°C)。化合物 **1** 的晶格包括(頭-尾)-相互作用二聚體，而化合物 **2** 的分子可能以π-π相互作用排列成重疊平面，但不存在 Pt···Pt 近距離接觸。化合物 **1** 和 **2** 在 400–500 nm 的低能紫外-可見範圍有具有負溶劑效應的中強吸收。兩個化合物在室溫的溶液中有壽命在微秒量級的強發光，該發射被認爲是 ^{3}[l → π*(二亞胺)](l = 孤對電子/酚鹽)與 ^{3}[Pt(d) → π*(二亞胺)]電荷轉移態的混合。採用時間-分辨吸收光譜研究化合物 **2** 的激發態性質并利用吡啶鹽受體淬滅實驗估算出了化合物 **2** 的激發態的氧化還原電勢。這些發光體還被用作多層 OLEDs 的電致磷光摻雜劑。混有化合物 **1** 和 **2** 器件在亮度，顏色，與總體表現上的差別可認爲是二亞胺取代基的影響。

Experimental Section

General: All chemicals were obtained from commercial sources and used as received. All reactions were performed under a nitrogen atmosphere and solvents for syntheses (analytical grade) were used without further purification. Solvents for photophysical measurements were purified according to conventional methods.[13] ^{1}H and ^{13}C NMR spectra were obtained on Bruker DRX 300, 500, and 600 FT-NMR spectrometers with tetramethylsilane (TMS) as reference. Mass spectra (FAB and EI) were obtained on a Finnigan Mat 95 mass spectrometer. Elemental analyses were performed by the Institute of Chemistry at Chinese Academy of Sciences, Beijing.

UV/Vis absorption spectra were obtained on a Perkin–Elmer Lambda 19 UV/Visible spectrophotometer. Steady-state emission spectra were recorded on a SPEX 1681 Fluorolog-2 series F111 spectrophotometer equipped with a Hamamatsu R928 PMT detector. Emission lifetimes were obtained with a Quanta Ray DCR-3 pulsed Nd:YAG laser system (pulse output 355 nm, 8 ns). Errors for λ (±1 nm), τ (±10%), and Φ (±10%) values are estimated. Further details of instrumentation and emission measurements have been given previously.[4a]

2,9-Bis(2′-methoxyphenyl)-4,7-diphenyl-1,10-phenanthroline: A solution of *o*-bromoanisole (15 g) in Et_2O (30 mL) was added in a dropwise fashion to a suspension of lithium metal pieces (2 g) in Et_2O (20 mL) under a nitrogen atmosphere. The mixture was refluxed for 2 h to yield a freshly prepared solution of *o*-lithioanisole. This was slowly added to an ice-cooled solution of 4,7-diphenyl-1,10-phenanthroline (4.4 g) in degassed toluene (50 mL), and a wine-red solution was obtained immediately. The resultant mixture was refluxed for 24 h and cooled in an ice bath, then deionized water (25 mL) was added to hydrolyze the products. The organic phase was separated and stirred with MnO_2 (50 g) for 24 h, then filtered and dried with $MgSO_4$. A pale yellow solid was obtained upon concentration of the solution, and this was collected by filtration, washed successively with MeOH and Et_2O, and dried under vacuum. Yield: 3.7 g (51%). ^{1}H NMR (300 MHz, [D$_6$]acetone): 8.41 (d, J = 7.6 Hz, 2H; C_6H_4), 8.29 (s, 2H; phen), 7.89 (s, 2H; phen), 7.54–7.7 (m, 10H; Ph), 7.49 (t, J = 7.8 Hz, 2H; C_6H_4), 7.16–7.25 (m, 4H; C_6H_4), 3.97 ppm (s, 6H; OMe); EI-MS: m/z: 544 $[M]^+$.

2,9-Bis(2′-hydroxyphenyl)-4,7-diphenyl-1,10-phenanthroline ($Ph_2N_2O_2H_2$): A mixture of the anisole precursor (2 g, 3.7 mmol) and pyridinium hydrochloride (4.23 g, 37 mmol) was heated under nitrogen at 210 °C for 36 h. After cooling, water (30 mL) was added and the aqueous solution was extracted with chloroform (3 × 30 mL). The combined organic extracts were washed with saturated sodium bicarbonate solution (5 × 30 mL) and water (3 × 30 mL), dried over magnesium sulfate, and evaporated to give a bright yellow solid. Chromatography on silica gel with n-hexane/dichloromethane (1:2) as eluent afforded a yellow solid. Yield: 0.99 g (52%). ^{1}H NMR (300 MHz, $CDCl_3$): 14.69 (s, 2H; OH), 8.22 (s, 2H; phen), 8.00 (d, J = 8.2 Hz, 2H; C_6H_4), 7.84 (s, 2H; phen), 7.58 (virtual s, 10H; Ph), 7.41 (t, J = 7.7 Hz, 2H; C_6H_4), 7.30 (d, J = 8.3 Hz, 2H; C_6H_4), 6.98 ppm (t, J = 7.5 Hz, 2H; C_6H_4); ^{13}C NMR (151 MHz, $CDCl_3$): 160.5, 157.7, 150.3, 142.8, 137.8, 132.2, 129.6, 128.9, 128.8, 127.1, 125.7, 123.7, 120.6, 119.4, 119.2, 118.9 ppm; FAB-MS: m/z: 517 $[M+H]^+$.

6,6′-Bis(2″-methoxyphenyl)-4,4′-bis(*tert*-butyl)-2,2′-bipyridine: The procedure for the 4,7-diphenyl-1,10-phenanthroline analogue was adopted by using 4,4′-di-*tert*-butyl-2,2′-bipyridine. Upon workup, a yellow oily substance was obtained. This was purified by chromatography on a silica gel column with petroleum ether (60–80 °C)/ethyl acetate (8:1) as eluent. The crude product was collected and recrystallized from hexane to give white

crystals. Yield: 3.3 g (35 %). ^{1}H NMR (300 MHz, $CDCl_3$): 8.47 (d, J = 1.8 Hz, 2H; bpy), 8.01 (d, J = 7.6, 2H; C_6H_4), 7.91 (d, J = 1.8 Hz, 2H; bpy), 7.40 (t, J = 7.8 Hz, 2H; C_6H_4), 7.15 (t, J = 7.4 Hz, 2H; C_6H_4), 7.05 (d, J = 8.2 Hz, 2H; C_6H_4), 3.90 (s, 6H; OMe), 1.42 ppm (s, 18H; *t*Bu); EI-MS: m/z: 479 $[M]^+$.

6,6′-Bis(2″-hydroxyphenyl)-4,4′-bis(*tert*-butyl)-2,2′-bipyridine (tBu$_2$N$_2$O$_2$H$_2$): A mixture of the anisole precursor (1 g) in hydrobromic acid (47 %, 20 mL) was refluxed for 12 h. This was cooled to room temperature and neutralized with a saturated Na_2CO_3 solution. The organic product was extracted with chloroform, washed with deionized water (2 × 50 mL), and dried over Na_2SO_4. A solid residue was obtained by removal of volatiles, and this was recrystallized from a methanol/dichloromethane solution to afford white crystals. Yield: 0.56 g (60 %). ^{1}H NMR (300 MHz, $CDCl_3$): 14.45 (s, 2H; OH), 8.16 (d, J = 1.4 Hz, 2H; bpy), 7.97 (d, J = 1.3 Hz, 2H; bpy), 7.90 (d, J = 8.0 Hz, 2H; C_6H_4), 7.34 (t, J = 8.4 Hz, 2H; C_6H_4), 7.07 (d, J = 8.2 Hz, 2H; C_6H_4), 6.96 (t, J = 8.1 Hz, 2H; C_6H_4), 1.47 ppm (s, 18H; *t*Bu); ^{13}C NMR (151 MHz, $CDCl_3$): 163.3 159.7, 157.5, 152.2, 131.5, 126.5, 119.2, 118.9, 118.4, 116.7, 116.4, 35.6, 30.6 ppm; EI-MS: m/z: 452 $[M]^+$.

Pt(Ph$_2$N$_2$O$_2$) (1): A mixture of K_2PtCl_4 (0.10 g, 0.25 mmol) and $Ph_2N_2O_2H_2$ (0.13 g, 0.25 mmol) was refluxed in glacial acetic acid (10 mL) for 48 h. After cooling, the resulting suspension was collected by filtration, washed with acetic acid and water, and dried under vacuum to afford a brown solid. The crude product was recrystallized by slow evaporation of a dichloromethane solution to afford red crystals. Yield: 0.11 g (62 %). ^{1}H NMR (400 MHz, CD_2Cl_2): 8.67 (s, 2H; phen), 8.36 (d, J = 8.8 Hz, 2H; C_6H_4), 8.02 (s, 2H; phen), 7.61 – 7.47 (m, 14H; Ph and C_6H_4), 6.88 ppm (m, 2H; C_6H_4); FAB-MS: m/z: 710 $[M]^+$; elemental analysis calcd (%) for $C_{36}H_{22}N_2O_2Pt\cdot 0.5\,CH_2Cl_2$: C 58.29, H 3.08, N 3.72; found: C 58.50, H 3.03, N 3.81.

Pt(tBu$_2$N$_2$O$_2$) (2): The same procedure was used as for **1**. The product was recrystallized by slow diffusion of diethyl ether into a dichloromethane solution to afford yellow crystals. Yield: 25 %. ^{1}H NMR (300 MHz, $CDCl_3$): 8.32 (d, J = 1.3 Hz, 2H; bpy), 8.01 (d, J = 8.5 Hz, 2H; C_6H_4), 7.86 (d, J = 1.7 Hz, 2H; bpy), 7.48 (d, J = 8.5 Hz, 2H; C_6H_4), 7.38 (t, J = 7.6 Hz, 2H; C_6H_4), 6.78 (t, J = 7.5 Hz, 2H; C_6H_4), 1.54 ppm (s, 18H; *t*Bu); ^{13}C NMR (151 MHz, $CDCl_3$): 162.7, 159.1, 155.3, 149.9, 131.3, 128.0, 124.1, 120.5, 120.4, 116.3, 36.0, 30.4 ppm; FAB-MS: m/z: 645 $[M]^+$; elemental analysis calcd (%) for $C_{30}H_{30}N_2O_2Pt$: C 55.81, H 4.68, N 4.34; found: C 55.39, H 4.70, N 4.14.

X-ray crystallography: Crystal data for **1**·CH_2Cl_2: $C_{37}H_{24}N_2O_2Cl_2Pt$, M_r = 794.57, triclinic, $P\bar{1}$, a = 8.481(2), b = 13.292(3), c = 14.024(3) Å, α = 71.48(3)°, β = 87.14(3)°, γ = 72.20(3)°, V = 1425.3(6) Å^3, Z = 2, ρ_{calcd} = 1.851 g cm^{-3}, $\mu(Mo_{K\alpha})$ = 5.150 mm^{-1}, $F(000)$ = 776, crystal size = 0.40 × 0.15 × 0.10 mm^3, T = 293(2) K, $2\theta_{max}$ = 50.7°, 4746 independent reflections (R_{int} = 0.032), 397 variable parameters, R_1 = 0.038 ($I > 2\sigma(I)$), wR_2 = 0.099, GOF(F^2) = 1.09, max./min. residual electron density 0.928/ − 2.373 e Å^{-3}. For **2**: $C_{30}H_{30}N_2O_2Pt$, M_r = 645.65, monoclinic, $P2_1/m$, a = 12.359(2), b = 6.9720(14), c = 14.438(3) Å, β = 93.12(3)°, V = 1242.2(4) Å^3, Z = 2, ρ_{calcd} = 1.726 g cm^{-3}, $\mu(MoK_\alpha)$ = 5.678 mm^{-1}, $F(000)$ = 636, crystal size = 0.50 × 0.20 × 0.03 mm^3, T = 301(2) K, $2\theta_{max}$ = 50.9°, 2074 independent reflections (R_{int} = 0.048), 205 variable parameters, R_1 = 0.044 ($I > 2\sigma(I)$), wR_2 = 0.112, GOF(F^2) = 1.12, max./min. residual electron density 1.559/ − 1.789 e Å^{-3}. Data collection was performed on an MAR diffractometer with a 300 mm image plate detector (λ = 0.71073 Å). Crysystallographic data (excluding structure factors) for the structures reported in this paper have been deposited with the Cambridge Crystallographic Data Centre as supplementary publications no. CCDC-193494 (**2**) and CCDC-193493 (**1**). Copies of the data can be obtained free of charge via www.ccdc.cam.ac.uk/conts/retrieving.html (or from the Cambridge Crystallographic Data Centre, 12 Union Road, Cambridge CB2 1EZ, UK; fax: (+44) 1223-336-033 or e-mail: deposit@ccdc.cam.ac.uk).

Device fabrication: ITO-coated glass slides (ITO = indium tin oxide) with a sheet resistance of 20 Ω/square were used as substrate and anode. Before loading into a deposition chamber, the ITO-coated glass slides were cleaned with organic solvents (toluene, acetone, and methanol) and deionized water, dried using an infrared oven, and finally treated with ultraviolet (uv)-ozone before use. Each device was assembled in sequence using the following materials: ITO electrode; hole-transport material *N*,*N*′-di(α-naphthyl)-*N*,*N*′-diphenyl-(1,1′-biphenyl)-4,4′-diamine (NPB) (thickness 300 Å); emitting layer composed of host material beryllium bis(2,2′-hydroxyphenyl)pyridine ($Bepp_2$) and emitting dopant (complex **1** or **2**) (thickness 300 Å); electron-injection layer of lithium fluoride (LiF) (thickness 5 Å), and aluminum layer as cathode (thickness 2500 Å).
The organic layers were laminated in sequence under 5×10^{-6} mbar without breaking vacuum between different vacuum deposition processes. The cathode metal was deposited in another chamber under 5×10^{-6} mbar vacuum immediately after organic deposition. The layers were deposited at rates of 2 – 5 Å s^{-1}. The emissive area of the devices as defined by the overlapping area of the cathode and anode was 3 × 3 mm^2. EL spectra and brightness-current density-voltage characteristics of the devices were measured in air at room temperature with a Spectroscan PR650 spectrophotometer and a computer-controlled direct-current power supply.

Results

Synthesis and characterization: The potentially tetradentate bisphenols $Ph_2N_2O_2H_2$ and tBu$_2$N$_2$O$_2$H$_2$ are derived from 4,7-Ph_2phen and 4,4′-tBu$_2$bpy, respectively, by modification of the literature preparation for 2,9-bis(2′-hydroxylphenyl)-1,10-phenanthroline.[14] By adapting the procedure reported by Scandola et al.[15] for Ptq_2, treatment of the ligands with K_2PtCl_4 in refluxing glacial acetic acid yielded the neutral platinum(II) complexes [Pt($Ph_2N_2O_2$)] (**1**) and [Pt(tBu$_2$N$_2$O$_2$)] (**2**) (Scheme 1). Although **1** is readily soluble only in DMF, CH_2Cl_2, and C_6H_6, the *tert*-butyl groups in **2** impart high solubility in most common organic solvents, except aliphatic hydrocarbons. These materials are indefinitely stable in the solid state but undergo partial decomposition in solution when exposed to light and atmospheric conditions. To examine their suitability for vacuum deposition processes during OLED fabrication, complexes **1** and **2** were studied by thermal gravimetric analysis (Figure 1), and both materials exhibited high thermal stability in nitrogen and air (heating rate 15 °C min^{-1}). Hence **1** and **2** are stable up to 440 and 530 °C, respectively, in N_2, while both undergo significant weight loss from around 380 °C in air.

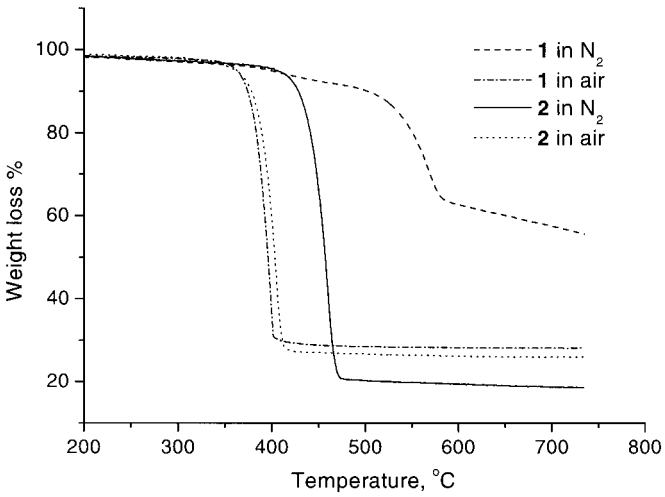

Figure 1. TGA thermograms of complexes **1** and **2** under nitrogen and air.

Crystal structures and packing: The molecular structures of complexes **1** and **2** were determined by X-ray crystallography (Figure 2, top). Several similarities, as well as important differences, are evident and are described below. The square-

0947-6539/03/0906-1266 $ 20.00+.50/0 *Chem. Eur. J.* **2003**, *9*, No. 6

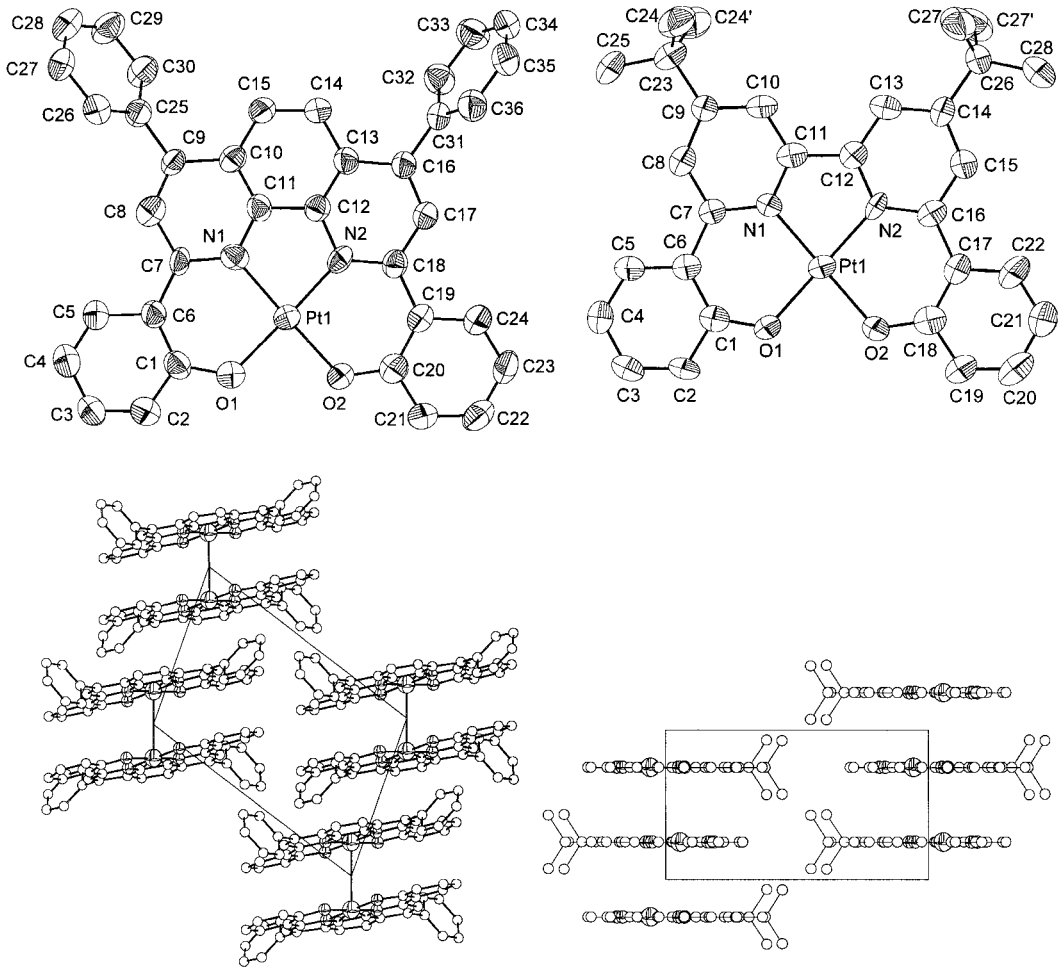

Figure 2. Perspective views (50 % thermal probability) and packing arrangements along the *ab* plane for **1** (left) and **2** (right). Selected bond lengths [Å] and angles [°] for **1**: Pt1–N1 1.978(6), Pt1–N2 1.941(6), Pt1–O1 1.983(6), Pt1–O2 1.972(5); Pt1–O1–C1 123.8(5), Pt1–O2–C20 124.1(5). For **2**: Pt1–N1 1.97(1), Pt1–N2 1.96(1), Pt1–O1 1.97(1), Pt1–O2 1.98(1); Pt1–O1–C1 123.4(9), Pt1–O2–C18 123(1).

planar geometry around the Pt cores and the Pt–N and Pt–O distances (mean 1.960 and 1.978 Å in **1** and 1.963 and 1.975 Å in **2**) are generally unremarkable. The central $Pt(N_2O_2)$ frameworks in both structures are highly planar. However, the two phenyl substituents of the phen ligand in **1** deviate significantly (47.8 and 70.7°) from the mean plane of the molecule, hence the Ph groups may not participate in π overlap with the phenanthroline moiety in the solid state. Close examinations of the crystal lattices of **1** and **2** reveal contrasting intermolecular contacts (Figure 2, bottom). Molecules of **2** form extended sheets that are stacked directly along the *c* axis, and the interplanar distance is equivalent to *b*/2, that is 3.486 Å. This allows the possibility of extended π-stacking interactions, but a view of the *ac* plane shows a noticeably displaced configuration and non-interacting metal centers (Pt ⋯ Pt 5.521 Å). In the crystal lattice of **1**, molecules are assembled into dimeric entities that are stacked in a head-to-tail manner. The $Pt(N_2O_2)$ planes of the dimers are separated by 3.462 Å, which is comparable to **2**. The distinctly eclipsed and overlapping dimeric arrangement and the closest Pt–Pt distance of 3.517 Å[16] in **1** may result in solid-state photo- and electroluminescent properties that are different from **2** (see below).

Electronic absorption and emission spectra: excited-state properties: The photophysical data of **1** and **2** are summarized in Table 1 and their UV/Vis absorption spectra in CH_2Cl_2 are depicted in Figure 3. Both derivatives exhibit intense high-energy absorptions at $\lambda_{max} < 375$ ($\varepsilon > 10^4\ mol^{-1}\,dm^3\,cm^{-1}$). In addition, moderately intense bands are observed at $\lambda_{max} = 420$ and (488 sh) 504 nm (5300 and ~7000 $mol^{-1}\,dm^3\,cm^{-1}$ respectively) for **1** and $\lambda_{max} = 397$ and 479 nm (504 sh) (8400 and ~2700 $mol^{-1}\,dm^3\,cm^{-1}$, respectively) for **2**. The effects of solvent polarity on the UV/Vis absorptions of **1** and **2** were investigated. While the energies of the absorption maxima for **2** at $\lambda \leq 315$ nm remain virtually unchanged, the low-energy absorption bands undergo significant blue shifts in solvents of greater polarity (λ_{max}): 408, 500 nm (533 sh) in C_6H_6/CH_2Cl_2 (10:1); 397, 479 nm (504 sh) in CH_2Cl_2; 390, 465 nm in CH_3CN; 385, 465 nm in CH_3OH (Figure 4). Likewise, the low-energy absorptions of **1** display similar shifts (λ_{max}): 438, (504 sh) 535 nm in C_6H_6; 420 and (488 sh) 504 nm in CH_2Cl_2; 420 and (478 sh) 502 nm in DMF.

The photoluminescent data of **1** and **2** in various media are listed in Table 1. Complexes **1** and **2** are highly luminescent in solution at 298 K and display a structureless emission in CH_2Cl_2 at $\lambda_{max} = 586$ and 595 nm, respectively (Figure 3), with

  0947-6539/03/0906-1267 $ 20.00+.50/0

Table 1. Photophysical data.

Complex	Medium	T, K	λ_{abs} [nm] (ε, $\times 10^4$ mol^{-1}dm^{3}cm^{-1})	λ_{em} [nm] (τ, μs; Φ_{em})
Pt($Ph_2N_2O_2$) (**1**)	C_6H_6	298	298 (2.50), 324 (2.68), 331(sh, 2.57), 363 (2.09), 384 (2.08), 438 (0.45), 504 (sh, 0.59), 535 (0.68)	599 (5.0; 0.58)
	CH_2Cl_2	298	291 (3.92), 315 (3.40), 325 (3.23), 352 (2.58), 375 (2.47), 420 (0.52), 488 (sh, 0.67), 504 (0.72)	586 (5.3; 0.6)
	DMF	298	292 (3.45), 317 (3.64), 326 (sh, 3.54), 353 (2.84), 376 (2.69), 420 (0.64), 478 (sh, 0.73), 502 (0.78)	589 (3.2; 0.45)
	thin film	298	-	651
	EtOH/MeOH (4:1)	77	-	555 (max, 13), 597
	solid	298	-	660 (2.0)
	solid	77	-	594 (max, 4.5), 644, 700
Pt($tBu_2N_2O_2$) (**2**)	C_6H_6/CH_2Cl_2 (10:1)	298	319 (1.69), 408 (0.773), 500 (0.240), 533 (sh, 0.203)	605 (1.7; 0.09)
	CH_2Cl_2	298	253 (4.10), 313 (1.84), 397 (0.840), 479 (0.294), 504 (sh, 0.252)	595 (1.9; 0.12)
	CH_3CN	298	250 (4.45), 315 (1.85), 390 (0.847), 465 (0.309)	596 (1.3; 0.06)
	MeOH	298	247 (4.59), 310 (1.92), 385 (0.859), 465 (0.317)	592 (1.1; 0.05)
	thin film	298	-	599
	EtOH/MeOH (4:1)	77	-	535 (max, 17), 575, 620
	solid	298	-	562, 593 (max, 1.5 and 0.3[a]), 656, 718
	solid	77	-	577 (max, 3.3 and 0.4[a]), 625, 682

[a] Bi-exponential decay.

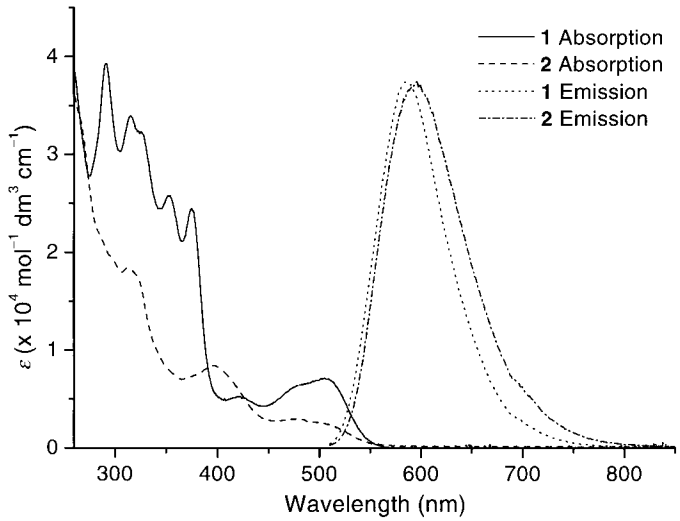

Figure 3. Absorption and emission (normalized, $\lambda_{ex} = 400$ nm) spectra of **1** and **2** in CH_2Cl_2 at 298 K.

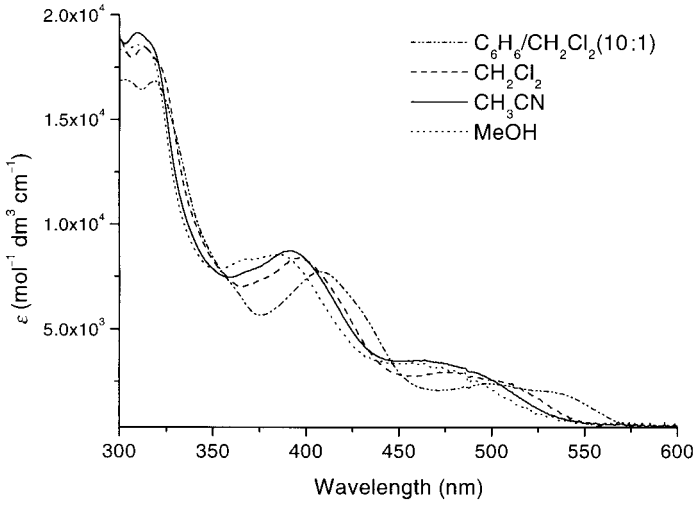

Figure 4. UV/Vis absorption spectra of **2** in various solvents at 298 K.

emission lifetimes and luminescent quantum yields of 5.3 μs and 0.6 for **1** and 1.9 μs and 0.1 for **2**. The time-resolved absorption-difference (TA) spectra for the excited state of **2** in various solvents at 298 K were obtained. Blue-shifted absorption peak maxima were observed from C_6H_6/CH_2Cl_2 (10:1) (450 nm) to CH_2Cl_2 (440 nm), and CH_3CN and CH_3OH (430 nm respectively; see Supporting Information for details and TA spectra in CH_3CN). For all of the solvents studied, the decay lifetimes (τ_{TA}) and emission lifetimes are in good agreement, indicating that the observed excited-state absorption can be ascribed to the excited state of **2**.

Upon examination, we found that the emission energies of **1** and **2** are influenced by solvent polarity. The emission maximum blue-shifts from 599 (in C_6H_6) to 586 (CH_2Cl_2), and 589 nm (DMF) for **1** and from 605 (in C_6H_6/CH_2Cl_2 (10:1)) to 595 (CH_2Cl_2), 596 (CH_3CN), and 592 nm (CH_3OH) for **2**. Compared with fluid solutions, the emissions of **1** and **2** in alcoholic glasses at 77 K are blue-shifted and highly structured. For example, the emission of **1** exhibits peak maxima at 555 and 597 nm (vibronic progression = 1270 cm^{-1}) and a lifetime of 13 μs. While the solid-state emissions of **1** and **2** are relatively diffused, the 77 K emissions are distinctly vibronic (progression about 1300 cm^{-1}). In this case, the emission of the Ph_2phen analogue **1** appears at partially lower energies (Figure 5).

To understand the excited-state reactivities and photoredox properties of the [Pt(N_2O_2)] complexes, it was beneficial to establish their excited-state redox potentials. This was performed for **2** by using spectroscopic and electrochemical data to estimate E^0[**Pt**$^{2+*/+}$] and E^0[**Pt**$^{3+/2+*}$] (**Pt** = **2**). The cyclic voltammogram of **2** shows irreversible reduction and oxidation waves at -1.94 and $+0.56$ V versus [Cp_2Fe]$^{+/0}$, respectively, in CH_2Cl_2. The irreversible nature of these electrochemical waves means that the excited-state reduction potential cannot be determined precisely. Therefore, quenching studies using a series of pyridinium acceptors [A$^+$] with different reduction potentials have also been employed.[17] A table listing the quenching data for **2** and the nonlinear least-

0947-6539/03/0906-1268 $ 20.00+.50/0 *Chem. Eur. J.* **2003**, *9*, No. 6

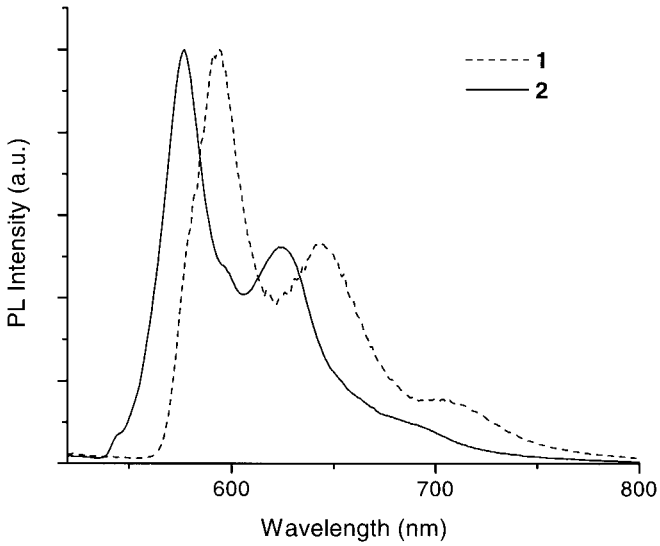

Figure 5. Normalized solid-state 77 K emission spectra of **1** and **2** (λ_{ex} = 355 nm).

square fitting of $\ln k_q'$ versus $E^0(A^+/A)$ using the Marcus equation (1) is provided in the Supporting Information.

$$(RT/F)\ln k_q' = (RT/F)\ln(K\kappa\nu) - [\lambda(1+\Delta G/\lambda)^2/4] \quad (1)$$

Here, $K = k_d/k_{-d}$ (which is approximately 1–2 $dm^3 mol^{-1}$) and κ, ν, and λ are the transmission coefficient, nuclear frequency, and reorganization energy for electron transfer, respectively; ΔG is the standard free-energy change for the reaction [Eq. (2)]; the work terms ω_p and ω_r associated with bringing the reactants/products to mean separation are small and are neglected.

$$\Delta G = E^0[\mathbf{Pt}^{3+/2+*}] - E^0(A^+/A) + \omega_p - \omega_r \quad (2)$$

Thus an excited-state reduction potential of -1.40 V versus SSCE (or -1.71 V versus $[Cp_2Fe]^{+/0}$) for $E^0[\mathbf{Pt}^{3+/2+*}]$ was calculated. This value closely corresponds to that (≤ -1.7 V versus $[Cp_2Fe]^{+/0}$) obtained from Equation (3), in which $E_{0\text{-}0}$ is approximated from the spectroscopic data (2.3 eV), and $E^0[\mathbf{Pt}^{3+/2+}]$ is estimated from the E_{pa} of the irreversible oxidation wave in cyclic voltammetry measurements (0.56 V versus $[Cp_2Fe]^{+/0}$). The large negative values obtained for $E^0[\mathbf{Pt}^{3+/2+*}]$ indicate that the excited state of **2** is strongly reducing.

$$E^0[\mathbf{Pt}^{3+/2+*}] = E^0[\mathbf{Pt}^{3+/2+}] - E_{0\text{-}0} \quad (3)$$

Electroluminescent properties: The photophysical properties and apparent stability of **1** and **2** signify that they are good candidates as phosphorescent emitters in organic electroluminescent (EL) devices. The following EL device structures were prepared: (ITO/NPB (300 Å)/**1** (or **2**) doped (x wt%) $Bepp_2$ (300 Å)/LiF (5 Å)/Al (2500 Å)) (devices A and B correspond to $Bepp_2$ layers doped with 2 and 10 wt% of complex **1** respectively; devices C–E correspond to $Bepp_2$ layers doped with 0.3, 1, and 2 wt% of complex **2**, respectively). Hence, the device structure is a multilayer stack deposited on ITO glass, and various EL devices at different doping concentrations of the platinum materials were fabricated. Bis(2-(2′-hydroxyphenyl)pyridine)beryllium ($Bepp_2$)[18] and *N*,*N*′-di(α-naphthyl)-*N*,*N*′-diphenyl-(1,1′-biphenyl)-4,4′-diamine (NPB) were employed as the host and hole-transporting layers respectively.

All devices exhibited low turn-on voltages of 5–7 V and generated yellow to yellow-green EL at various voltages. In device A, at 2% ratio of **1**, only the $Bepp_2$ emission at around 450 nm was observed when driven under forward bias. When the dopant concentration level of **1** was increased to 10% in device B, the resultant yellow EL was dominated by **1** at λ_{max} 588 nm. The EL of this device and the involvement from $Bepp_2$ was found to be voltage-dependent (Figure 6). Namely, the $Bepp_2$ emission at 444 nm was insignificant below 8 V, but slowly became observable at voltages above 8 V. Maximum luminance and power efficiency of 850 $cd\,m^{-2}$ (at 360 $mA\,cm^{-2}$) and 0.26 $lm\,W^{-1}$ (at 14 $mA\,cm^{-2}$), respectively, were achieved (see Supporting Information).

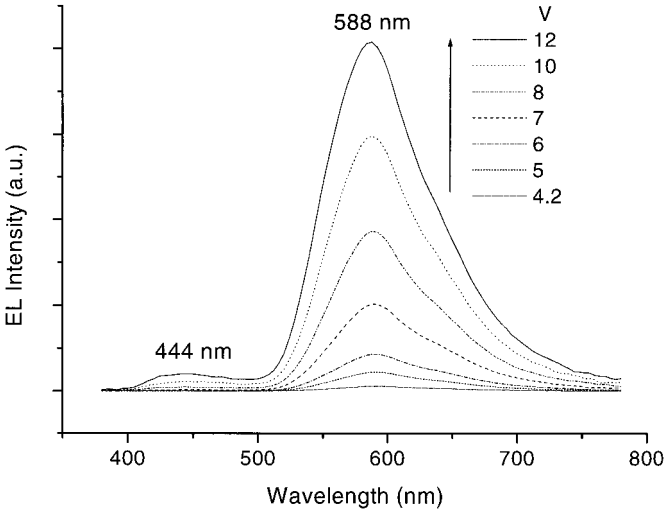

Figure 6. Voltage-dependent EL for [ITO/NPB/**1**-doped (10%) $Bepp_2$/LiF/Al].

The EL spectra of devices C–E are depicted in Figure 7. The EL spectrum of device C (0.3% of **2**) displayed two peaks at λ_{max} = 453 and 540 nm, due to emission from $Bepp_2$ and **2** respectively, that culminated in strong yellow-green EL (CIE 0.33, 0.47). Saliently, maximum luminance (Figure 8) and power efficiency of 9330 $cd\,m^{-2}$ (at 330 $mA\,cm^{-2}$) and 1.44 $lm\,W^{-1}$ (at 40 $mA\,cm^{-2}$), respectively, were detected. Upon enhancing the concentration of **2** to 1% in device D, the 550 nm emission from **2** became noticeably more intense than the $Bepp_2$ emission at 450 nm. However, this EL color adjustment (CIE 0.39, 0.54) was accompanied by detrimental device performance. For example, the maximum luminance dropped to 6200 $cd\,m^{-2}$ at 390 $mA\,cm^{-2}$ while the optimum efficiency fell to 0.80 $lm\,W^{-1}$ at 84 $mA\,cm^{-2}$.

In device E, a 2% dopant content of **2** generated yellow EL (CIE 0.42, 0.56) with minimal contribution from $Bepp_2$ emission, but the observed optimal luminance (4480 $cd\,m^{-2}$ at 280 $mA\,cm^{-2}$) and power efficiency (0.51 $lm\,W^{-1}$ at 280 $mA\,cm^{-2}$) were comparatively poor. The EL band shape

  0947-6539/03/0906-1269 $ 20.00+.50/0

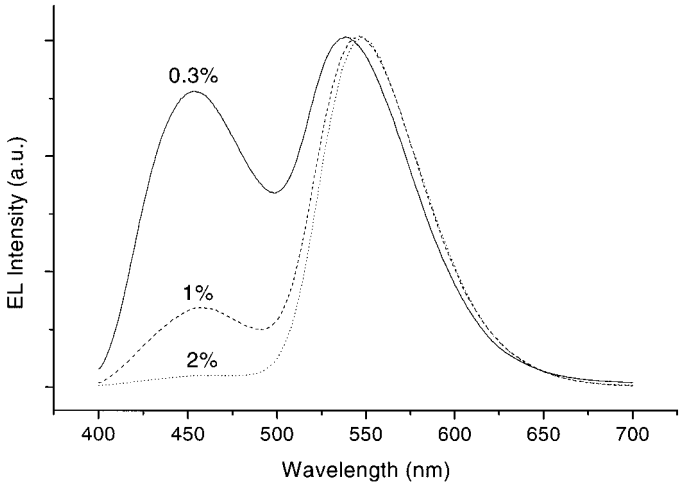

Figure 7. EL spectra for devices C–E: [ITO/NPB/**2**-doped (x%) $Bepp_2$/LiF/Al].

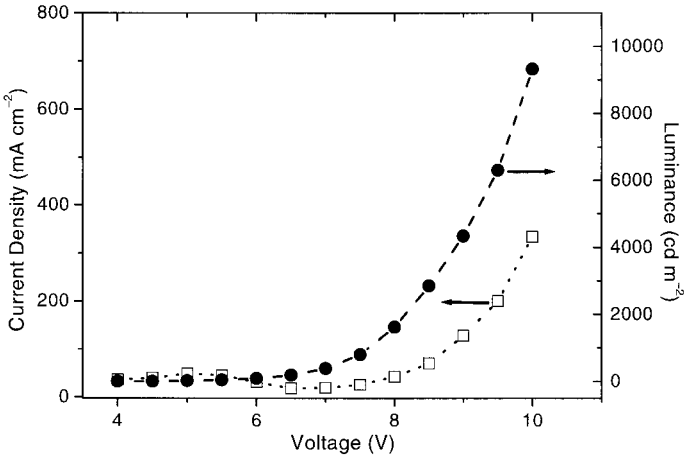

Figure 8. I-V-L characteristics for device C: [ITO/NPB/**2**-doped (0.3%) $Bepp_2$/LiF/Al].

is similar to the corresponding thin-film photoluminescence at $\lambda_{max} = 599$ nm but the EL energy ($\lambda_{max} = 548$ nm) is blue-shifted.

Discussion

Singlet and triplet states: The intense absorptions in the high-energy region ($\lambda < 375$ nm) of the UV/Vis spectra of complexes **1** and **2** are assigned to ligand-centered $^1(\pi\pi^*)$ transitions by comparison with the corresponding bisphenol ligands in CH_2Cl_2. However, the origins of the moderately intense absorptions at $\lambda_{max} = 420$ and 504 nm (488 sh) for **1** and $\lambda_{max} = 397$ and 479 nm (504 sh) for **2** are more problematic to elucidate. These absorption bands are clearly too low in energy for $\pi\pi^*$ transitions (the free ligands absorb very weakly at $\lambda > 370$ nm). We have plotted the absorbance of **2** at 510 nm against complex concentration and shown that this band obeys Beer's law, so the possibility of involvement by oligomeric species may be eliminated.

At this juncture, it is appropriate to discuss the photophysical and electronic nature of the closely related bischelate Ptq_2, which was first investigated in detail by Scandola et al.[15] and more recently by Yersin et al.[19] In DMF solution, Ptq_2 exhibits a low-energy band at 478 nm ($\varepsilon \approx 6900$ mol^{-1} dm^3 cm^{-1}). Because corresponding transitions appear at higher energies for Alq_3 and Rhq_3 ($\lambda_{max} = 388$ and 425 nm respectively), a metal-perturbed, ligand-centered $^1(l \rightarrow \pi^*)$ (l = lone pair/phenoxide) charge-transfer assignment was proposed[15] and later confirmed by Shpol'skii spectroscopic measurements.[19]

Because the absorption maxima, bandshape, and intensity of the low-energy bands for Ptq_2 and especially **2** bear great resemblance, we tentatively assign the low-energy absorptions at 400–500 nm in **1** and **2** to a $^1[l \rightarrow \pi^*(\text{diimine})]$ CT transition mixed with $Pt(d) \rightarrow \pi^*(\text{diimine})$ ^{1}MLCT. Furthermore, like Ptq_2, **1** and **2** also display negative solvatochromic shifts (the absorption of **2** at 24500 cm^{-1} (408 nm) in C_6H_6/CH_2Cl_2 (10:1) blue-shifts to 26000 cm^{-1} (385 nm) in MeOH), and this is consistent with the polar character of the electron-rich oxygen/phenoxide fragment in the ground state. We suggest that mixing with the ^{1}MLCT state is likely, and indeed, the energies of the absorptions for **1** and **2** at 420 and 397 nm, respectively, are typical of ^{1}MLCT transitions in Pt^{II} diimine complexes.[11, 20]

Finally, it is noteworthy that the above assignment is in essence equivalent to the $S(p)/Pt(d) \rightarrow \pi^*(\text{diimine})$ (i.e. 'charge-transfer-to-diimine') assignment designated by Eisenberg for the lowest energy absorption band in a related family of Pt^{II} diimine derivatives containing aromatic dithiolate ligands.[21] For example, the CT absorption for [Pt(4,4'-tBu$_2$bpy)(toluene-3,4-dithiolate)] appears at $\lambda_{max} = 563$ nm ($\varepsilon \approx 7200$ mol^{-1} dm^3 cm^{-1}) in CH_2Cl_2 and similarly undergoes negative solvatochromic shifts.[22]

The long emission lifetimes for **1** and **2** (in the μs range) strongly indicate phosphorescence. In general, the structureless emissions of **1** and **2** undergo blue shifts on cooling from 298 to 77 K and become highly structured. Vibronic progressions of about 1300 cm^{-1} are evident in the 77 K solid-state emission spectra and this is emblematic of $^3\pi\pi^*$ excited states for monomeric Pt^{II} diimine compounds.[23] However, the room-temperature fluid emissions of **1** and **2** are excessively red-shifted for this assignment. In addition, the negative solvatochromism observed for the PL of **1** and **2** is also inconsistent with a "normal" $^3\pi\pi^*$ state. By comparison with the emission spectra of Ptq_2 in absolute EtOH at 77 K ($\lambda_{max} = 625$, 680 nm; progression ≈ 1300 cm^{-1}), the equivalent spectra of **1** and **2** in glassy EtOH/MeOH are blue-shifted but the bandshape for **1** is remarkably similar and all three complexes display matching vibronic progressions. We therefore tentatively assign the emissions of **1** and **2** to mixed ^{3}MLCT and $^3[l \rightarrow \pi^*(\text{diimine})]$ (l = lone pair/phenoxide) excited states.

Electrophosphorescence and substituent effects: The tolerance of complexes **1** and **2** to heat and vacuum deposition conditions is thought to arise from the strong chelate effect and the chemically inert nature of the N_2O_2 ligand. The novel beryllium(II) chelate $Bepp_2$ (Hpp = 2(2'-phenol)pyridine) was recently employed by Wang and co-workers as an emitting layer in high-performance blue OLEDs[18a] and as a host material for the construction of orange-red light EL devices.[18b]

0947-6539/03/0906-1270 $ 20.00+.50/0 *Chem. Eur. J.* **2003**, *9*, No. 6

In the devices containing complex **1** as dopant, only EL from $Bepp_2$ was observed at 2% (device A), suggesting ineffective host–dopant Förster energy transfer. However, this would be surprising because there is excellent overlap between the host-emission and dopant-absorption spectra, so the shorter-range Dexter process is presumably dominant in the $Bepp_2$:**1** system. At 10% dopant level of **1** (device B), yellow EL from **1** only was visible at low voltages but contribution from the $Bepp_2$ host became noticeable around 10 V (Figure 6). This is consistent with the long electrophosphorescent lifetime exhibited by **1**, which leads to saturated triplet exciton population at high voltages so that energy transfer from $Bepp_2$ excitons becomes blocked. While the abundance of π electrons in **1** may be beneficial for charge mobility, the favorable formation of dimeric assemblies (see crystal lattice of **1**) and the presence of pendant phenyl substituents can facilitate intermolecular quenching (including self-quenching) processes. This may explain the inferior brightness and efficiency of devices derived from dopant **1**.

The employment of ancillary ligands containing bulky substituents has been demonstrated to be advantageous for electrophosphorescent OLEDs with regards to the suppression of self-quenching activities[24] and the maintenance of amorphous films.[25] In this work, modification of the diimine fragment from Ph_2phen in **1** to t-Bu_2bpy in **2** results in substantially improved OLED performance. At 0.3% dopant level of **2**, (device C), long-range Förster energy transfer from host excitons appears considerably more efficient compared to **1** and EL from **2** at $\lambda_{max} = 540$ nm is observed, although the $Bepp_2$ emission at 450 nm remains prominent. Excellent maximum luminance (9330 cd cm^{-2}) and power efficiency (1.44 lm W^{-1}) have been realized, and this can be ascribed to the molecular structure of **2**, which may mediate effective charge transport to yield relatively balanced charge recombination within the **2**-doped $Bepp_2$ layer without promoting quenching mechanisms.

A device that produces EL from **2** only was targeted. When the concentration of **2** was increased to 2%, the $Bepp_2$ emission is drastically reduced and the EL from **2** became dominant. However, this was achieved at the expense of diminished device function, which may be accredited to enhanced aggregation of dopant molecules leading to intermolecular quenching (see continuously stacked layers in crystal lattice of **2**) or formation of crystalline domains. In summary, the overall brightness and performance of devices derived from the *tert*-butyl substituted complex **2** is superior to those using the phenyl derivative **1**. While the performances of these devices have yet to be optimized, it is our intention in this work to highlight the potential merit of this class of electrophosphorescent materials in OLED applications.

Acknowledgements

We are grateful for financial support from the University of Hong Kong, the Croucher Foundation (Hong Kong), Research Grants Council of Hong Kong SAR, China [HKU 7298/99P], and the Innovation and Technology Commission of the Hong Kong SAR Government (ITS/053/01). We also thank Dr. S. C. Yu for technical assistance.

[1] M. A. Baldo, D. F. O'Brien, Y. You, A. Shoustikov, S. Sibley, M. E. Thompson, S. R. Forrest, *Nature* **1998**, *395*, 151–154.

[2] a) J. Kido, H. Hayase, K. Hongawa, K. Nagai, K. Okuyama, *Appl. Phys. Lett.* **1994**, *65*, 2124–2126; b) S. Hoshino, H. Suzuki, *Appl. Phys. Lett.* **1996**, *69*, 224–226; c) X. Zhang, R. Sun, Q. Zheng, T. Kobayashi, W. Li, *Appl. Phys. Lett.* **1997**, *71*, 2596–2598; d) Y. Ma, H. Zhang, J. Shen, C. M. Che, *Synth. Met.* **1998**, *94*, 245–248; e) M. D. McGehee, T. Bergstedt, C. Zhang, A. P. Saab, M. B. O'Regan, G. C. Bazan, V. I. Srdanov, A. J. Heeger, *Adv. Mater.* **1999**, *11*, 1349–1354.

[3] a) D. F. O'Brien, M. A. Baldo, M. E. Thompson, S. R. Forrest, *Appl. Phys. Lett.* **1999**, *74*, 442–444; b) V. Cleave, G. Yahioglu, P. Le Barny, R. H. Friend, N. Tessler, *Adv. Mater.* **1999**, *11*, 285–288; c) C. Adachi, M. A. Baldo, S. R. Forrest, S. Lamansky, M. E. Thompson, R. C. Kwong, *Appl. Phys. Lett.* **2001**, *78*, 1622–1624.

[4] a) S. C. Chan, M. C. W. Chan, Y. Wang, C. M. Che, K. K. Cheung, N. Zhu, *Chem. Eur. J.* **2001**, *7*, 4180–4189; b) W. Lu, B. X. Mi, M. C. W. Chan, Z. Hui, N. Zhu, S. T. Lee, C. M. Che, *Chem. Commun.* **2002**, 206–207.

[5] a) M. A. Baldo, S. Lamansky, P. E. Burrows, M. E. Thompson, S. R. Forrest, *Appl. Phys. Lett.* **1999**, *75*, 4–6; b) M. A. Baldo, M. E. Thompson, S. R. Forrest, *Nature* **2000**, *403*, 750–753; c) Y. Wang, N. Herron, V. V. Grushin, D. LeCloux, V. Petrov, *Appl. Phys. Lett.* **2001**, *79*, 449–451; d) C. Adachi, R. C. Kwong, P. Djurovich, V. Adamovich, M. A. Baldo, M. E. Thompson, S. R. Forrest, *Appl. Phys. Lett.* **2001**, *79*, 2082–2084; e) S. Lamansky, P. Djurovich, D. Murphy, F. Abdel-Razzaq, H.-E. Lee, C. Adachi, P. E. Burrows, S. R. Forrest, M. E. Thompson, *J. Am. Chem. Soc.* **2001**, *123*, 4304–4312; f) X. Gong, M. R. Robinson, J. C. Ostrowski, D. Moses, G. C. Bazan, A. J. Heeger, *Adv. Mater.* **2002**, *14*, 581–585.

[6] a) C. Adachi, M. A. Baldo, S. R. Forrest, M. E. Thompson, *Appl. Phys. Lett.* **2000**, *77*, 904–906; b) C. Adachi, M. A. Baldo, M. E. Thompson, S. R. Forrest, *J. Appl. Phys.* **2001**, *90*, 5048–5051; c) M. Ikai, S. Tokito, Y. Sakamoto, T. Suzuki, Y. Taga, *Appl. Phys. Lett.* **2001**, *79*, 156–158; d) B. W. D'Andrade, J. Brooks, V. Adamovich, M. E. Thompson, S. R. Forrest, *Adv. Mater.* **2002**, *14*, 1032–1036.

[7] a) C. W. Tang, S. A. VanSlyke, *Appl. Phys. Lett.* **1987**, *51*, 913–915; b) C. W. Tang, S. A. VanSlyke, C. H. Chen, *J. Appl. Phys.* **1989**, *65*, 3610–3616.

[8] a) C. H. Chen, J. Shi, *Coord. Chem. Rev.* **1998**, *171*, 161–174; b) J. Kido, Y. Iizumi, *Appl. Phys. Lett.* **1998**, *73*, 2721–2723; c) L. S. Sapochak, A. Padmaperuma, N. Washton, F. Endrino, G. T. Schmett, J. Marshall, D. Fogarty, P. E. Burrows, S. R. Forrest, *J. Am. Chem. Soc.* **2001**, *123*, 6300–6307.

[9] P. E. Burrows, L. S. Sapochak, D. M. McCarty, S. R. Forrest, M. E. Thompson, *Appl. Phys. Lett.* **1994**, *64*, 2718–2720.

[10] a) T. A. Hopkins, K. Meerholz, S. Shaheen, M. L. Anderson, A. Schmidt, B. Kippen, A. B. Padias, H. K. Hall, Jr., N. Peyghambarian, N. R. Armstrong, *Chem. Mater.* **1996**, *8*, 344–351; b) N. Donzé, P. Péchy, M. Grätzel, M. Chaer, L. Zuppiroli, *Chem. Phys. Lett.* **1999**, *315*, 405–410; c) L. S. Sapochak, F. E. Benincasa, R. S. Schofield, J. L. Baker, K. K. C. Riccio, D. Fogarty, H. Kohlmann, K. F. Ferris, P. E. Burrows, *J. Am. Chem. Soc.* **2002**, *124*, 6119–6125.

[11] a) H. Kunkely, A. Vogler, *J. Am. Chem. Soc.* **1990**, *112*, 5625–5627; b) K. T. Wan, C. M. Che, K. C. Cho, *J. Chem. Soc. Dalton Trans.* **1991**, 1077–1080; c) W. B. Connick, D. Geiger, R. Eisenberg, *Inorg. Chem.* **1999**, *38*, 3264–3265; d) S. W. Lai, M. C. W. Chan, T. C. Cheung, S. M. Peng, C. M. Che, *Inorg. Chem.* **1999**, *38*, 4046–4055; e) W. Lu, M. C. W. Chan, K. K. Cheung, C. M. Che, *Organometallics* **2001**, *20*, 2477–2486.

[12] a) R. C. Kwong, S. Sibley, T. Dubovoy, M. A. Baldo, S. R. Forrest, M. E. Thompson, *Chem. Mater.* **1999**, *11*, 3709–3713; b) R. C. Kwong, S. Lamansky, M. E. Thompson, *Adv. Mater.* **2000**, *12*, 1134–1138.

[13] D. D. Perrin, W. L. F. Armarego, D. R. Perrin, *Purification of Laboratory Chemicals, 2nd ed.*, Pergamon, Oxford, **1983**.

[14] S. Routier, V. Joanny, A. Zaparucha, H. Vezin, J.-P. Catteau, J.-L. Bernier, C. Bailly, *J. Chem. Soc. Perkin Trans.* **1998**, 863–868.

[15] R. Ballardini, G. Varani, M. T. Indelli, F. Scandola, *Inorg. Chem.* **1986**, *25*, 3858–3865.

[16] This falls at the outer limit of the range of intermetal distances (2.7–3.5 Å) reported in 'monomeric' platinum(II) extended-linear-chain structures: a) J. J. Novoa, G. Aullón, P. Alemany, S. Alvarez, *J. Am.*

Chem. Soc. **1995**, *117*, 7169 – 7171; b) J. S. Miller, A. J. Epstein, *Prog. Inorg. Chem.* **1976**, *20*, 1 – 151.
[17] J. L. Marshall, S. R. Stobart, H. B. Gray, *J. Am. Chem. Soc.* **1984**, *106*, 3027 – 3029.
[18] a) Y. Liu, J. Guo, J. Feng, H. Zhang, Y. Li, Y. Wang, *Appl. Phys. Lett.* **2001**, *78*, 2300 – 2302; b) Y. Li, Y. Liu, W. Bu, D. Lu, Y. Wu, Y. Wang, *Chem. Mater.* **2000**, *12*, 2672 – 2675.
[19] D. Donges, J. K. Nagle, H. Yersin, *Inorg. Chem.* **1997**, *36*, 3040 – 3048.
[20] W. B. Connick, V. M. Miskowski, V. H. Houlding, H. B. Gray, *Inorg. Chem.* **2000**, *39*, 2585 – 2592.
[21] S. D. Cummings, R. Eisenberg, *Inorg. Chem.* **1995**, *34*, 2007 – 2014.
[22] S. D. Cummings, R. Eisenberg, *J. Am. Chem. Soc.* **1996**, *118*, 1949 – 1960.
[23] V. M. Miskowski, V. H. Houlding, C. M. Che, Y. Wang, *Inorg. Chem.* **1993**, *32*, 2518 – 2524.
[24] H. Z. Xie, M. W. Liu, O. Y. Wang, X. H. Zhang, C. S. Lee, L. S. Hung, S. T. Lee, P. F. Teng, H. L. Kwong, Z. Hui, C. M. Che, *Adv. Mater.* **2001**, *13*, 1245 – 1248.
[25] J. C. Ostrowski, M. R. Robinson, A. J. Heeger, G. C. Bazan, *Chem. Commun.* **2002**, 784 – 785.

Received: September 17, 2002 [F4433]

  0947-6539/03/0906-1272 $ 20.00+.50/0